Mississippi State University
Scholars Junction

Theses and Dissertations | Theses and Dissertations

1-1-2012

Effects of Thermo-Mechanical and Thermal Treatments on the Structure-Property Relationships of Dual Phase (DP) and Transformation-Induced Plasticity (TRIP) steels

Matthew Leonard Jones

Follow this and additional works at: https://scholarsjunction.msstate.edu/td

Recommended Citation

Jones, Matthew Leonard, "Effects of Thermo-Mechanical and Thermal Treatments on the Structure-Property Relationships of Dual Phase (DP) and Transformation-Induced Plasticity (TRIP) steels" (2012). *Theses and Dissertations*. 1811.
https://scholarsjunction.msstate.edu/td/1811

This Graduate Thesis - Open Access is brought to you for free and open access by the Theses and Dissertations at Scholars Junction. It has been accepted for inclusion in Theses and Dissertations by an authorized administrator of Scholars Junction. For more information, please contact scholcomm@msstate.libanswers.com.

Effects of thermo-mechanical and thermal treatments on the structure-property relationships of dual phase (DP) and transformation-induced plasticity (TRIP) steels

By

Matthew Leonard Jones

A Thesis
Submitted to the Faculty of
Mississippi State University
in Partial Fulfillment of the Requirements
for the Degree of Master of Science
in Mechanical Engineering
in the Department of Mechanical Engineering.

Mississippi State, Mississippi

December 2012

Copyright 2012

By

Matthew Leonard Jones

Effects of thermo-mechanical and thermal treatments on the structure-property relationships of dual phase (DP) and transformation-induced plasticity (TRIP) steels

By

Matthew Leonard Jones

Approved:

Hongjoo Rhee Assistant Research Professor of Mechanical Engineering (Co-Major Professor)	Mark Horstemeyer Professor of Mechanical Engineering (Co-Major Professor)
Haitham El Kadiri Assistant Professor of Mechanical Engineering (Committee Member)	Steven Daniewicz Department Head and Professor of Mechanical Engineering (Graduate Coordinator)
Sarah Rajala Dean of the College of Engineering	

Name: Matthew Leonard Jones

Date of Degree: December 15, 2012

Institution: Mississippi State University

Major Field: Mechanical Engineering

Major Professors: Hongjoo Rhee, Mark Horstemeyer

Title of Study: Effects of thermo-mechanical and thermal treatments on the structure-property relationships of dual phase (DP) and transformation-induced plasticity (TRIP) steels

Pages in Study: 48

Candidate for Degree of Master of Science

The investigation of thermo-mechanical and thermal treatments on the microstructure and mechanical behavior of DP590 and TRIP680 steels revealed several critical aspects of the materials' responses to different testing. Various thermo-mechanical treatments were carried out to identify the responses to the said treatments. Following these preconditioning protocols, quasi-static, and high strain-rate tests showed how the materials reacted under tensile testing to fracture. Ensuing heat treatments on the as-received materials were performed to bring about phase fraction changes to each of the steels. These heat-treated DP and TRIP steels were examined to discover microstructural characteristics and mechanical responses through quasi-static and high strain-rate testing. The responses of the steels were analyzed and compared to the as-received testing results to observe the significant changes of mechanical behavior that occurred.

DEDICATION

Without the support and motivation from my parents, Leonard and Kathy Jones, none of this would be possible. This thesis, which most likely its contents do not interest you whatsoever, is dedicated to you two. Thank you for all that you have done in order to turn my dreams into realities.

ACKNOWLEDGEMENTS

First and foremost, I would like to acknowledge and give thanks to my major professor, Dr. Hongjoo Rhee, for all of his help and insight with this project. His advice, enthusiasm, and more importantly patience was critical in my reaching this point in my academic career. I would then like to thank my committee members Dr. Mark Horstemeyer and Dr. Haitham El Kadiri. Their willingness to work with me and serve on my committee is very beneficial because people of their level of knowledge help make it possible for this to become a quality report. In addition, Dr. Bin Li's guidance with the x-ray diffraction analysis was crucial in completing the heart of this project.

Secondly, I would like to thank everyone downstairs in lab services for their eagerness to teach me how to use all of the laboratory machines to help my project progress in an efficient matter. Because the majority of this project is experimental and lab-based, Stephen Horstemeyer, Melissa Mott, and Robert Malley all were very willing to work with me so that I may learn proper techniques and perform the tasks at hand to the best of my ability. Furthermore, I would like to thank Wilburn Whittington and Scott Turnage for their help on the high strain-rate testing.

I would also like to thank our industrial partners, Severstal and POSCO, for providing this project with the quality materials that enabled this project to move forward. In addition, the U.S. Department of Energy's funding for this project made this research possible.

TABLE OF CONTENTS

Page

LIST OF TABLES

LIST OF FIGURES

LIST OF ACRONYMS

MPa	*MegaPascals*
DP steel	*Dual Phase steel*
DP590	*Dual Phase steel with 590 MPa tensile strength*
TRIP	*Transformation-Induced Plasticity*
TRIP680	*Transformation-Induced Plasticity steel with 680 MPa tensile strength*
AHSS	*Advanced High-Strength Steels*
CP steel	*Complex Phase stees*
MS	*Martensitic Steels*
HSLA	*High-Strength Low-Alloy Steels*
CCT	*Continuous Cooling Transformation*
SEM	*Scanning Electron Microscopy*
Hv	*Vickers hardness value*
SHB	*Split Hopkinson Bar*
XRD	*X-ray Diffraction*
I.C.A.	*Intercritical Annealing*
RT	*Room Temperature*

CHAPTER I

INTRODUCTION

The desire for increasing fuel efficiency and safer automobiles is as much of a concern with automobile manufacturers as it ever has been [1–3]. The compositional design of a novel steel with lower mass, increased strength, and retained workability with the capability to retain strength following fabrication is the challenge that the steel industry constantly faces. One solution to this problem is the implementation of advanced high strength steels (AHSS), specifically transformation-induced plasticity (TRIP) steels and dual phase (DP) steels. Despite their advantageous characteristics, high strength steels have manufacturing issues due to inherently resisting deformation and wearing of tooling [4]. These steels have received increasing attention to improve manufacturability, strength, and decrease weight [5].

Steel automotive body sheets are stamped, or press-formed, into body panels. After this process the steel must maintain its high strengths. This characteristic of the material is called formability. One of the most important objectives in the development of the automotive steel sheet is the combination of strength and formability [6]. In order to keep the material at its lowest possible strength during stamping, the carbon atoms in the steel sheet are kept in the solid solution condition. The press forming introduces dislocations in the steel consequently causing increased strength due to the work-hardening phenomenon. Subsequent manufacturing processes include painting and baking. During these steps, the panel is heated to around 170^{o}C which coins the term

baking. During baking, carbon atoms dissolved into the steel from the press-forming diffuse and segregate into the regions around the dislocations caused in the preceding step. This is usually carried out for 25 to 30 minutes.

The category of steels labeled first generation AHSS consist of steels such as TRIP, DP, Martensitic Steel (MS), and Complex Phase (CP) steels as seen in Figure 1.1 [7]. The most widely used of these steels are DP steels due to their simplistic microstructure composed of ferrite and martensite and the steel's cooling schedule. They are cost effective and exhibit mechanical behavior desired in automotive bodies. On the other hand, TRIP steels are beginning to increase in popularity due to their advantageous microstructural behavior under strain. Having an untransformed microstructure of ferrite, bainite, and retained austenite, these TRIP steels undergo a phase change when exposed to certain strains transforming retained austenite to a harder and stronger martensite [8].

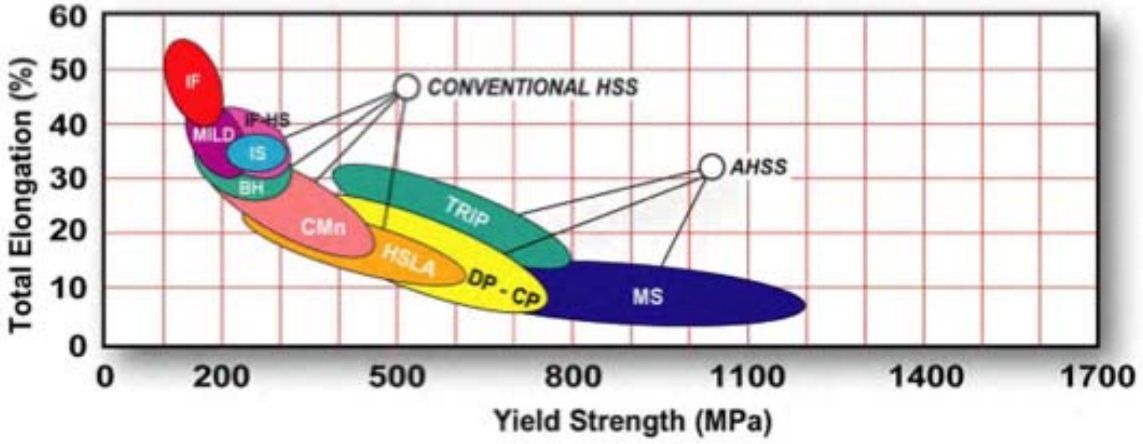

Figure 1.1 Depiction of AHSS (in color) in regard to strength and elongation compared to conventional steels (in grey).

DP steel can be created in one of two ways: intercritical annealing of cold-rolled sheets or full austenization, both followed by controlled cooling from the peak treating

temperature [9]. Rapid cooling causes austenite to transform to martensite during the cooling process creating the dual-phase microstructure [10]. Carbon content is critical at this stage due to the fact the carbon atoms stabilize the retained austenite through cooling. The end result is a ferrite-martensite matrix designed to have ample energy absorbability due to the ferrite while having the ability to obstruct strain waves during deformation which gives it the increased work hardening rate [11]. Different cooling patterns allow the volume fraction of the microstructure to be altered that result in different mechanical properties.

The microstructure of TRIP steel is obtained after an intercritical annealing or full austenization and a resulting isothermal annealing in the bainitic transformation region, called austempering [12]. Retained austenite is simply austenite that was not transformed to martensite during quenching. In steels with greater than 0.3% carbon or various alloying elements, M_f is usually below room temperature so this retained austenite remains untransformed at room temperature [13]. The stability of the retained austenite through the cooling process has been proven to enhance the strength and work hardening behavior of the steel [14]. The capability of TRIP steels exhibit an improved blend of ductility and strength compared to precipitation and solution hardened steels [15]. TRIP steels are somewhat new industrially and incorporate the phenomenon of retained austenite transforming to martensite with increasing strain thereby increasing the work hardening rate at higher strain levels which increases the ductility of the steel. The fact that TRIP steel resists local necking improves its formability by increasing the high strain hardening ability [16]. Previous research suggests that TRIP steels demonstrate cyclic hardening due to the internal stresses [17]. Due to the martensitic transformation, this can result in crack closure and thus the crack growth rate may be controlled and reduced.

TRIP steel has a distinct advantage over other advanced high strength steels when comparing strain hardening and ultimate tensile strength. The added work hardening allows for the TRIP steels to have significant stretch-forming whereas other high strength steels sometimes come up short in that area [18]. Studies have shown that the TRIP effect significantly enhances strength and ductility by delaying the plastic localization due to a high work hardening rate [19].

AHSS classifications usually are designated by tensile strengths and/or yield strengths along with elongation of the material [7]. Work-hardening, the level of stretchability measured by the work hardening exponent (n), plays a pivotal role in designing an alloy for automotive body due to the necessary formability and energy-absorption. Since stamping causes displacements in the steel, total elongation has long been the standard for measuring stretchability of a material but the more recent trend is to use the n-value.

The automotive industry is demanding a steel alloy with the microstructure that results in the material having higher elongations, an increased n-value, ample energy absorption, and most importantly cost-effective. Formability is still the most decisive factor when choosing the most applicable steel to use for the automobile. Thus, the newly desired 3rd gen. AHSS will be achieved finding the right blend of chemical composition, microstructure, and thermomechanical properties. The main objective of this experimental study on the two AHSS is to perform methodical research to determine the corresponding behavior of the two materials when dealing with strain-rate variations. This investigation will aid in the experimental progression of 1st gen to 3rd gen. AHSS resulting in steel with maintained higher strengths while increasing elongation abilities with the novel steel. In addition, this is in correspondence with the discovery of the

effects of thermal and thermo-mechanical treatments on the microstructures and mechanical properties of the examined steels.

CHAPTER II

DUAL PHASE STEEL

2.1 Introduction

The ferrite-martensite microstructure that is DP steel provides for a tailorable balance of strength and ductility. Martensite's higher carbon content and BCT structure allow for it to be the backbone of the steel giving its rigidity and higher strengths. The ferrite phase gives the steel its ductility and elongation. The two phases combine to create a microstructure shown in the schematic below in Figure 2.1 [7].

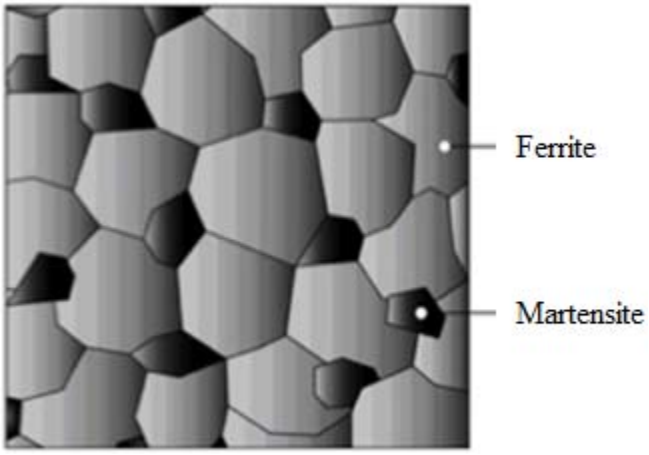

Figure 2.1 Schematic of DP steel showing the interspersed phases of ferrite and martensite.

Tensile tests, both quasi-static and high strain-rate, along with various heat treatments were carried out in order to discover how the properties alter the behavior of the steel. The knowledge gained from these tests allow for the development of situation-specific steels in order to create the most desirable dual phase steel from

2.2 Experimental Procedures

With the continued thought of designing a novel AHSS in mind, DP steels were investigated by studying the microstructures, mechanical properties, and typical manufacturing processes. For the purpose of truly understanding the behavior, various tests were carried out on DP steel where the output and resultant knowledge is directed at the future automotive design efforts.

To begin, chemical compositions were obtained to determine the amounts of different alloying elements in the steel with a SPECTROMAXx chemical spectrometer. Optical images were obtained by mounting, grinding, and mechanical polishing followed by etching with 2% nital. Scanning electron microscopy (SEM) images were obtained through scanning electron microscopy (SEM) with a Zeiss EVO 50 scanning electron microscope. Microstructural images were and through conventional optical microscopy with a Zeiss Axiovert 200 optical microscope. Area phase fractions were found by image analysis software. Vickers hardness values were obtained through a LECO LR300TD hardness tester in order to observe the overall properties of the steel. A load of 10gf was applied in the Vickers hardness tests.

To understand the larger perspective of the mechanical properties of the steel, which aspects include yield strength, tensile strength, work hardening exponent (n-value), strain-rate consequences, etc., tensile tests were performed at various strain rates. Specimens were pre-strained on an Instron EM Model 5882 Compression/Tension testing system and then baked at a temperature of 175^{o}C for 25 minutes. The baked specimens were only prescribed to the baking process after being pre-strained in order to simulate the stamping-then-baking manufacturing process. Therefore, later where graphs denote "Pre-strained and baked," this refers to the material being pre-strained, removed from the

tensile testing machine, baked in a muffle furnace, and then cooled to room temperature. Quasi-static specimens were preconditioned in the schedule shown below in Table 2.1. Strain-rate controlled quasi-static tensile tests were performed on the same Instron testing system used in pre-straining. For the quasi-static testing, 0.001/s and 0.01/s strain rates were used.

Table 2.1 Schedule of the quasi-static and high strain-rate tensile tests

	As Rec.	**1% Pre-strain**	**2% Pre-strain**	**5% Pre-strain**
Un-treated	X			
Baked	X	X	X	X

High strain-rate tests were performed on a split Hopkinson Bar (SHB) testing apparatus as shown in Figure 2.2 at strain rates of approximately 500/s [20]. A SHB testing apparatus is constructed of two bars, 7075 aluminum in this case, called the incident and transmitted bars. These bars resonate strain waves recorded by strain gages placed on the bars. Upon placing load on the incident bar which will deliver the fatal tensile force, a breaker pin is used to hold the incident bar in place while strain is placed upon it. Once the desired strain is achieved, pressure is applied to the breaker pin. Upon fracture of the breaker pin, the incident bar retracts, as a consequence, in turn fracturing the specimen held by the transmitted bar. The initial strain wave propagates from the incident bar through the specimen at fracture into the transmitted bar. The strain waves are recorded and then analyzed to find the correct stress-strain curves.

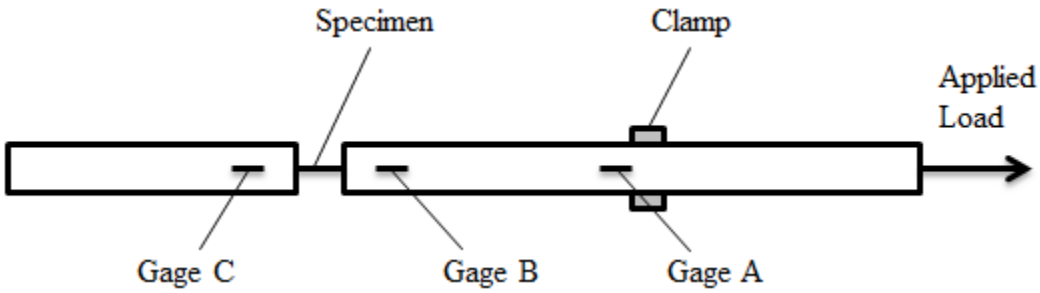

Figure 2.2 Schematic of tension SHB high strain-rate testing apparatus.

Various heat treatments were performed on the obtained DP590 in order to investigate the fractional changes of ferrite and martensite in the microstructure. Specimens were fully austenized at 925^{o}C and then cooled at different temperatures of 720^{o}C, 760^{o}C, and 800^{o}C in muffle furnaces as shown in the schematic in Figure 2.3. Then each specimen was quenched in three different media: oil, water, and ice-brine. In order to determine area fractions, the steels were mounted, grinded, polished, and etched for observation of microstructures under optical and SEM microscopes. The thermal treatment that revealed the most martensite percentage and ferrite percentage was carried out on tensile specimens and then tested at the quasi-static regime. The treatment with the most martensite percentage was also tested in tension under high strain-rates (approximately 500/s).

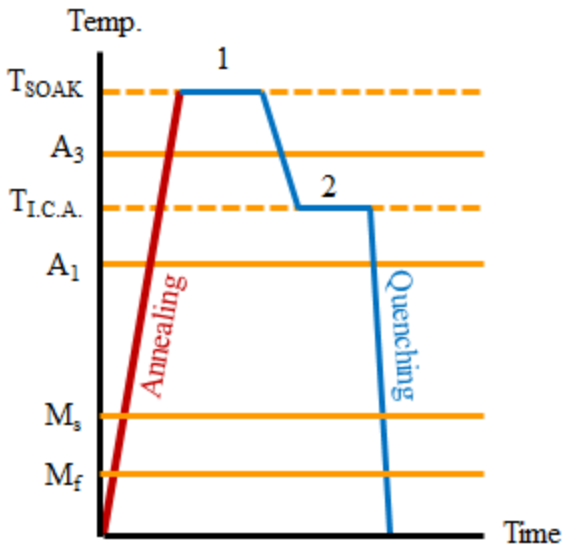

Figure 2.3 Heating/cooling schematic for the creation of DP steel.

2.3 Results and Discussion

2.3.1 Examination of the Microstructure, Chemical Composition, and Microhardness of the As-received DP590.

Chemical composition was taken through spectroscopy, and the results are shown in Figure 2.4. Noted manganese content serves as block for the formation of pearlite and the silicon helps prevent Fe_3C development. Polishing and etching revealed the ferrite-martensite phase fraction as seen in Figure 2.5. The martensitic phases can be seen interspersed through the ferrite.

C	Si	Mn	P	S	Cr	Mo	Al
0.123	0.103	1.870	0.013	0.0046	0.008	0.061	0.049

Figure 2.4 Chemical composition of as-received DP590.

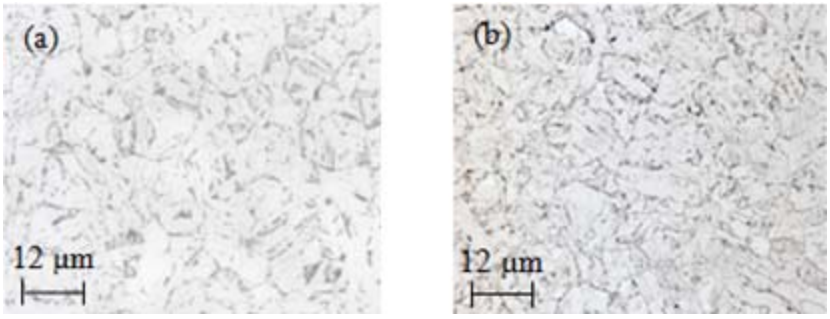

Figure 2.5 Microstructure of acquired DP steel.

Note: Ferrite (light grey) and martensite (dark grey/black) are shown with top surface view (a) and side surface view (b).

Regarding the microhardness values, Vickers tests were performed on each phase in order to find out their mechanical properties. A 10 gf load was used in and the tests were carried out at room temperature. Ferrite provided values of Hv193 while martensite showed Hv295. Martensite is overwhelmingly harder due to higher carbon content and resultant BCT microstructure. Indents are shown below in Figure 2.6.

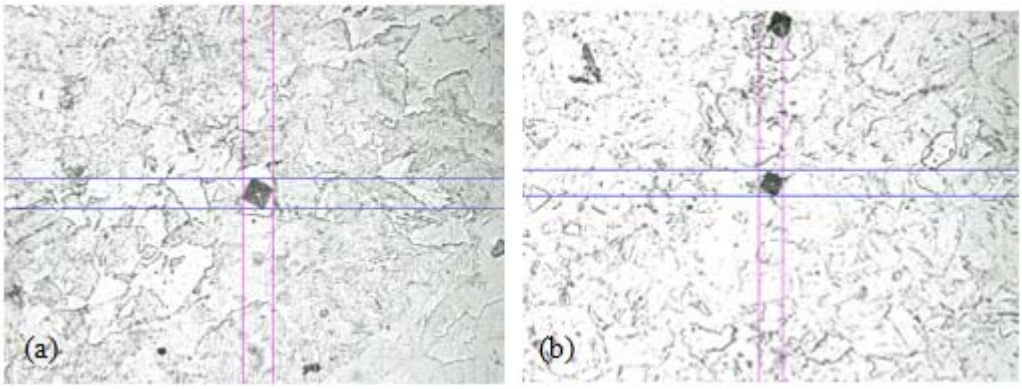

Figure 2.6 Vickers hardness indents showing indents on each phase of the steel.

Note: (a) the ferritic region produced a mean hardness value of Hv193; (b) the martensitic region produced a mean hardness value of Hv295.

2.3.2 Investigation into the Thermo-mechanical Preconditioning Effects on the Mechanical Behavior DP590

Quasi-static tests revealed slower strain-rate thermo-mechanical properties about the DP590. Tests were performed at 0.01/s and 0.001/s strain-rates with as-received and baked specimens under their respective pre-strainings mentioned in Table 2.1. The trend regarding ultimate tensile strength (UTS) appeared to be that the smaller the pre-strain, the higher the UTS. However, the specimens with the highest yield strength turned out to be the moderately pre-strained test cases. Therefore it can be deduced that the preconditioning of the test specimens controls the different stress criterion. Figure 2.7 shows the stress-strain curves from the quasi-static tests.

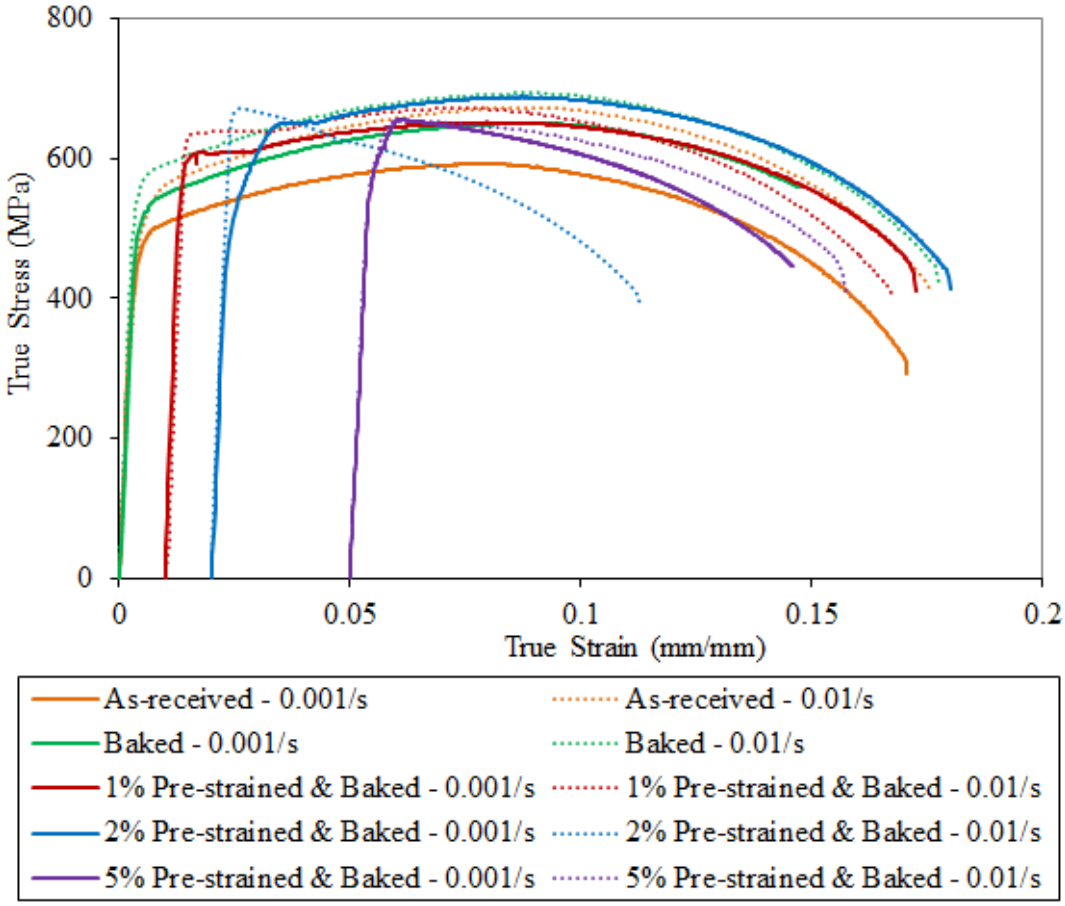

Figure 2.7 True stress vs. true strain curves from quasi-static tensile tests.

From the quasi-static tests, characteristics such as work-hardening and bake-hardening properties can be found and evaluated. This is useful in determining just how much the preconditioning protocols affected the material during these tests. It can be noted that the work-hardening effect increased due directly to the increasing pre-strains shown in Figure 2.8.

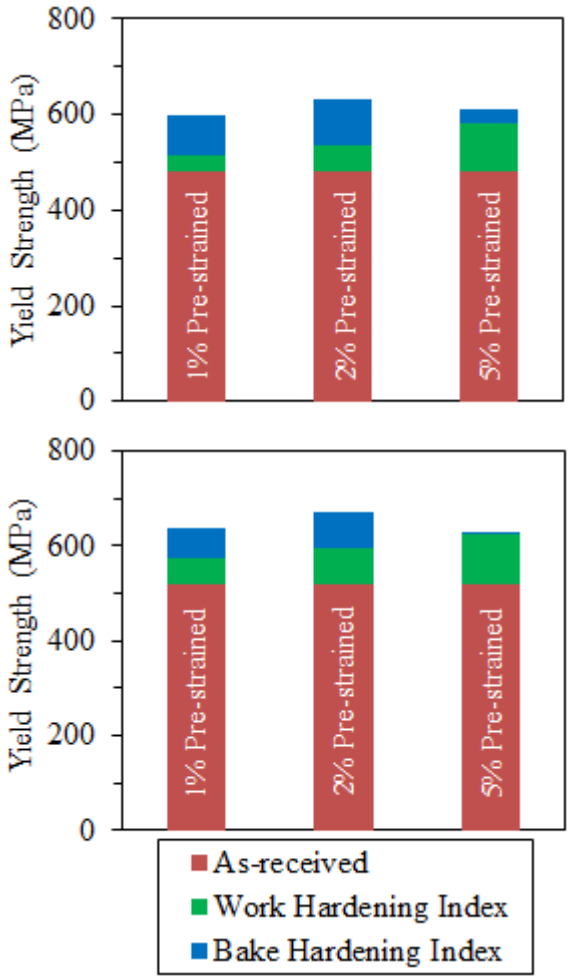

Figure 2.8 Work- and bake-hardening indices for their respective quasi-static tests. Note: (a) 0.001/s strain rate; (b) 0.01/s strain rate.

2.3.3 Heat-Treating and the Resultant Microstructures and Mechanical Behavior

Heat treatments were carried out with different intercritical annealing (I.C.A.) parameters coupled with different quenching media. Figure 2.9 shows the area fractions of martensite and ferrite in the different tests. Martensite percentages were observed to increase with the increase of the cooling rate (i.e., oil vs. water/ice) and also the increase of the annealing temperatures. However, there is no discernible difference in using an ice-brine quench compared to a water quench.

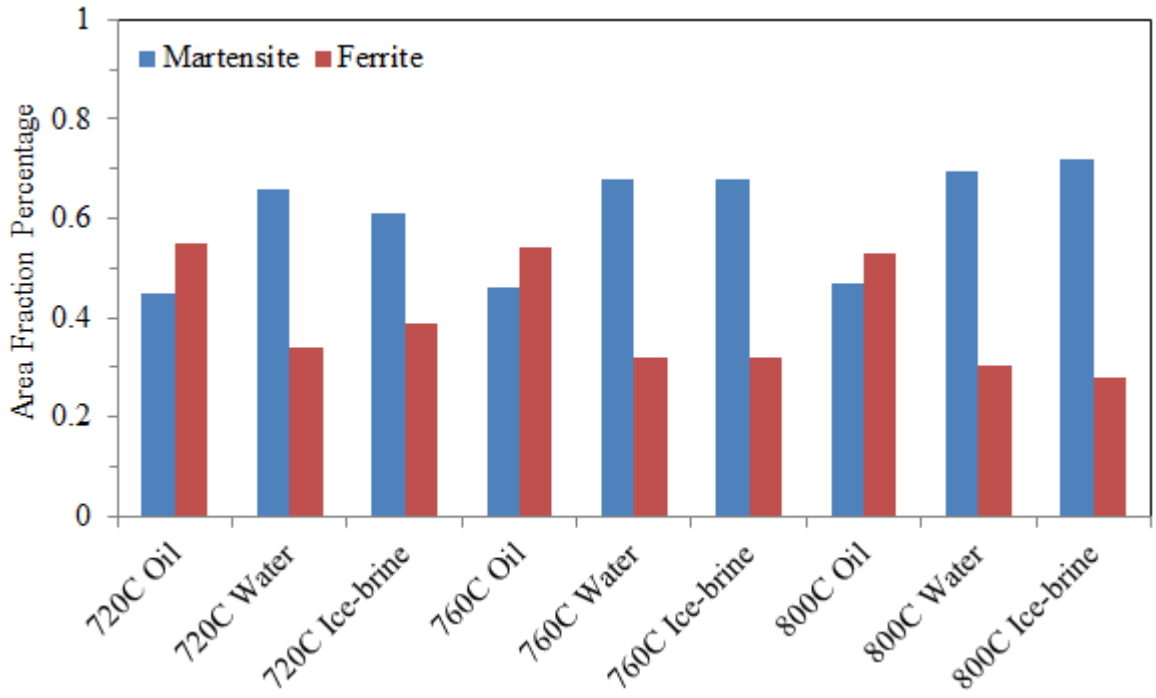

Figure 2.9 Area fractions of martensite and ferrite in different quenching cases.

Note: The annealing/quenching case that contains the highest ferrite percentage is 720°C/oil while the highest martensite percentage is 800°C/ice-brine

The two heat/quench treatments with the most martensite percentages and most ferrite percentages were used to make new specimens for another round of thermo-mechanical tests. Quasi-static tests were performed on the specimens that had undergone

annealing temperature/quenching media of 720°C/oil and 800°C/ice-brine. Figure 2.10 shows these results compared to the as-received DP590 series obtained from the supplier. It is evident that the material with the most martensite had the most tensile and yield strength, but reducing elongation-to-failure in effect causing more brittle behavior. The test case with the highest percentage of ferrite had a much better elongation to failure, similar to the as received series, but sacrificed strength in the process. These results can be contributed to the behavior of the microstructures of each material.

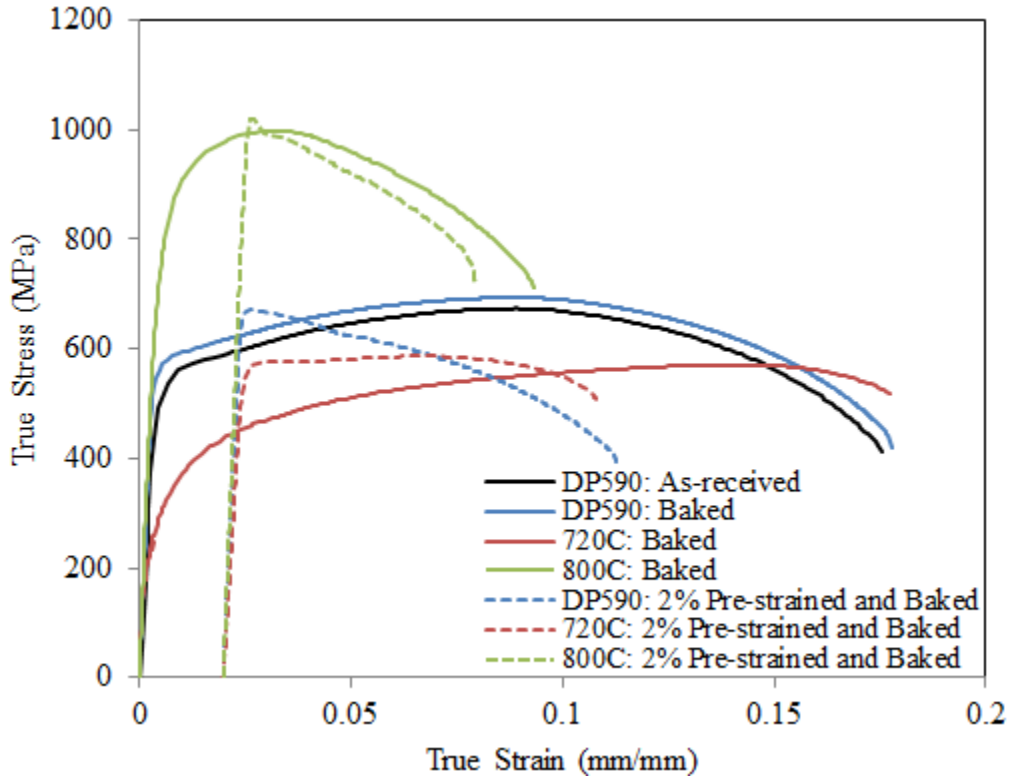

Figure 2.10 Quasi-static stress vs. strain results comparing the three different tempering cases at un-strained and 2% pre-strains tested at 0.01/s strain-rate.

The baking process of the as-received material induced only a very slight increase of the yield probably due to fine precipitation of carbon which was still in solid solution. The intercritical annealing at 720°C produced a microstructure with substantially lower

yiled stress (320 MPa vs. 600 MPa) as martensite fraction was considerably reduced. Uniform elongation and elongation to failure was, however, enhanced, which actually elucidates the detrimental effect of martensite on ductility. The fracture surface in 2.10 revealed damage progression by nucleation, growth, and coalescence of voids.

The annealing at 800^{o}C which mostly produces austenite, and thus, martensite after quenching, induced a marked increase in yield stress up to 1000 MPa. This marked increase in yield stress was accompanied by a dramatic reduction of ductility. The fracture surface in Figure 2.11 (c) indicates localized plastic deformation at the center of the specimen and probably nucleation of two shear bands which moved toward both edges of the specimen.

When pre-strained and baked, both steels pretreated at 720^{o}C and 800^{o}C showed a significant increase in yield stress and a decrease in ductility. However, the decrease in ductility for the steel annealed at 800^{o}C was characterized by a sharper peak which is characteristic of dramatic plastic instability. The fracture surface indicates a brittle fracture on a plane which was nearly normal to the stress axis. This indicates an anisotropic behavior of shear localization which was observed previously in martensitic steels [21]. Actually, both non-treated and 720^{o}C treated steels showed, after pre-strain and baking, kinks in the stress-strain curves immediately after yielding. The kinks correspond to mild yield point effects which are characteristic of shear band formation.

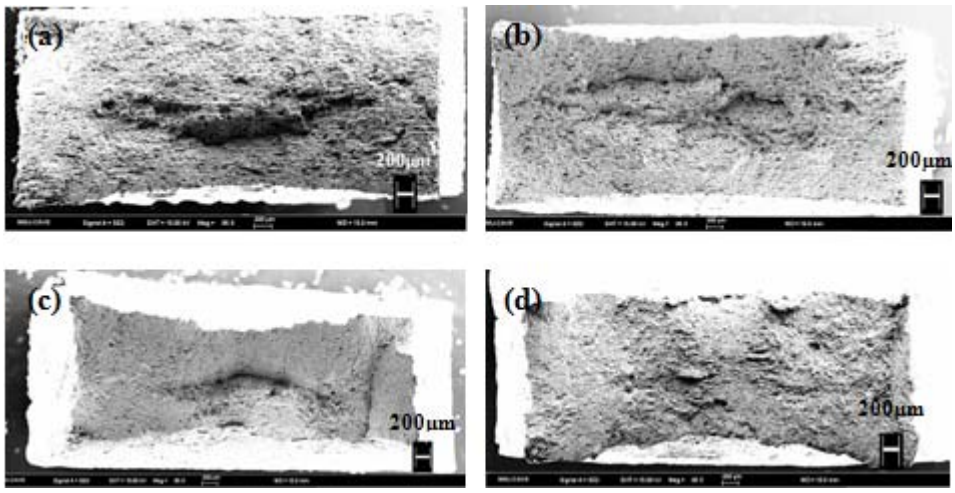

Figure 2.11 SEM fractography revealing fracture surfaces on the annealed series resulting from quasi-static testing.

Note: (a) 720°C annealed and oil quenched, (b) 720°C annealed and oil quenched then being 2% pre-strained and baked, (c) 800°C annealed and ice-brine quenched, (d) 800°C annealed and ice-brine quenched then being 2% pre-strained and baked.

Figure 2.12 shows stress vs. strain curves resulting from high strain-rate tensile tests on untreated series and the series 800°C/ice-brine. The test results revealed that the 1% pre-strained-and-baked series had the highest yield out of the received series although it is noted that there was not a significant difference in it and the received baked series. When comparing these tests with the heat-treated series, the heat-treated series was over 30 percent stronger than the strongest of the as-received series; however, the elongation to failure was reduced. As in the quasi-static tests, the 800°C/ice-brine series performed in much more of a brittle manner which was to be expected due to the higher fraction of martensite in the steel. Comparing the high strain-rate tests to the quasi-static tests, there does not seem to be much strain-rate sensitivity observed. Tensile strengths correlated between the two different tests similarly.

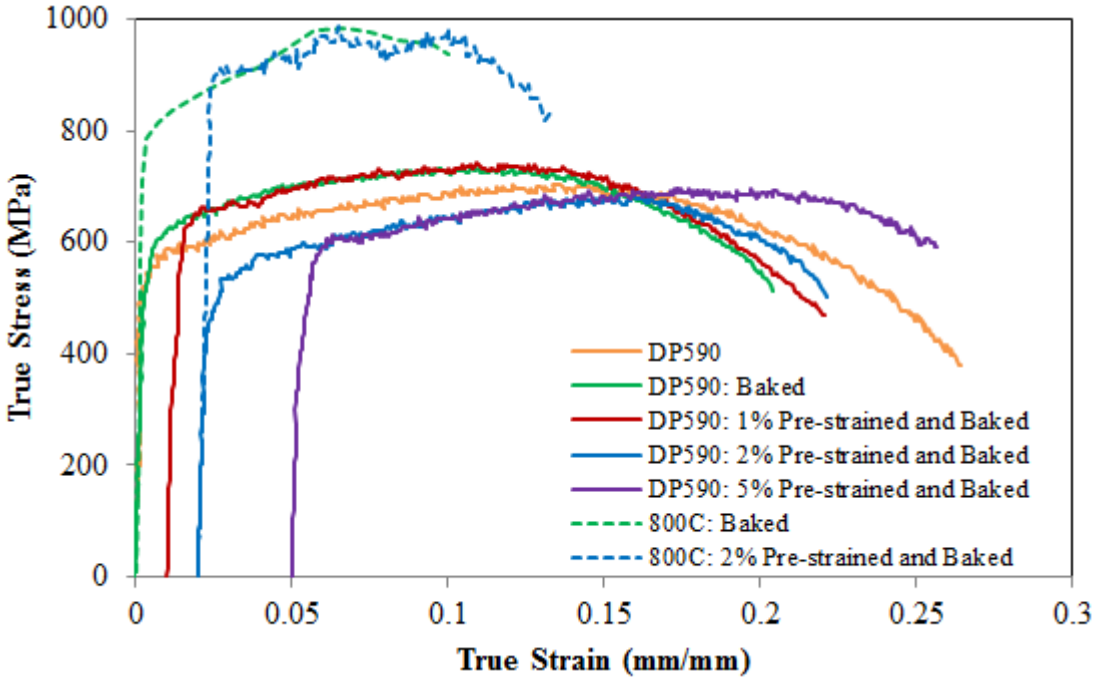

Figure 2.12 Stress versus strain curves resulting from high strain-rate tensile tests

Note: Strain rates of approximately 500/s were executed on the as-received series of specimens and 800°C-ice brine-cooled specimens with pre-straining and baking protocols particular to each individual specimen series.

CHAPTER III

TRIP STEEL

3.1 Introduction

The strength-ductility balance of TRIP steels is a result of complex heat-treatment schedule resulting in the microstructure comprising ferrite, bainite, retained austenite, and martensite, if so desired. The two-stage holding times for trapping ferrite and bainite are a critical part of the thermal treatments. However, the slow-cooling stage for retaining austenite in the steel proves to be the most critical step in the process because it is the austenite that is transformed into martensite upon deformation. The end result is a TRIP steel with a microstructure typical of the one shown below in Figure 3.1 [7].

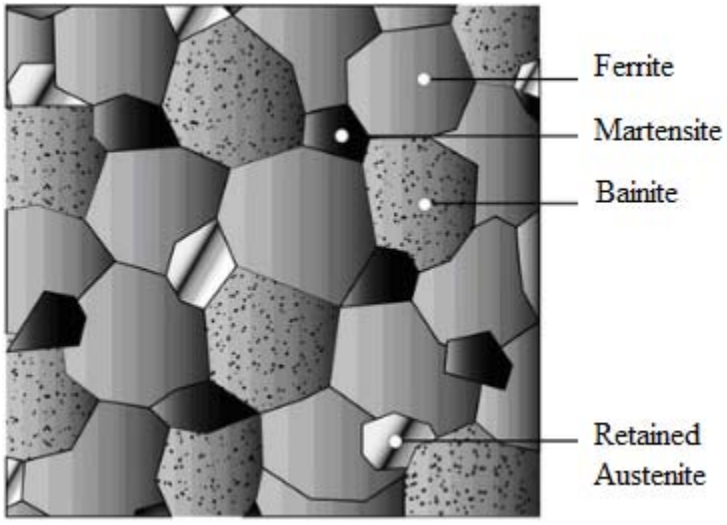

Figure 3.1 Schematic of TRIP steel showing the ferrite dominant matrix with phases of martensite, bainite, and retained austenite interspersed throughout.

Mechanical testing and heat treatments were conducted to determine the heat schedules for resultant steels and their specific mechanical behavior. The data gathered and knowledge gained will allow for TRIP steels to be specifically tailored to each individual situation in which it is desired to be used.

3.2 Experimental Procedures

In order to keep on the path for the design of a third generation AHSS, thermo-mechanical and microstructural evaluations were performed on TRIP680 steel obtained from Severstal of North America. With the purpose of determining microstructural behavior and their effects on quasi-static and high-rate tests with various heat treatments, similar test schedules were established to those in the DP steel investigation.

Spectroscopy analysis was performed by a SPECTROMAXx and confirmed by a Thermo-Electron ARL3460 Optical Emission Spectrometer through an industrial partner, Severstal. Ensuing microstructural evaluations followed. Grinding, polishing, and etching techniques using Beraha's tint etch for iron and steel were used in order to obtain visuals for the microstructure of the steel [22]. In order to be precise of the quantity of phases in the steel, XRD analyses were performed with a Rigaku Smartlab x-ray diffractometer. Bainite phases were determined through optical image analysis. Ferrite and austenite were determined via x-ray diffraction (XRD) through the direct comparison method [23] (see appendix).

Next, quasi-static tests were performed on an Instron EM Model 5882 Compression/Tension testing system and then baked at a temperature of 175^{o}C for 25 minutes. Consequently, the area volume fractions were quantified via XRD to give a foundation to compare the microstructural changes following testing. Next, high strain-

rate tests were performed for the same reasons except for observation under higher strain rates. Table 3.1 shows the test schedule protocols executed prior to quasi-static and high strain-rate tests.

Table 3.1 Test schedule of the quasi-static and high-rate testing of the acquired TRIP 680.

	As Rec.	**1% Pre-strain**	**2% Pre-strain**	**5% Pre-strain**
Un-treated	X			
Baked	X	X	X	X

Heat treatments were carried out on the steel to recreate the microstructure with varying area volume fractions with the cooling schematic shown in Figure 3.2. In two cases, full austenization was achieved followed by annealing in the intercritical region, thermal holding in the bainitic region, followed by air cooling to room temperature (RT). Cooling of the material was performed by removing the specimens from the furnaces and holding at RT until the desire temperature was reached. The next series was conducted by peaking at intercritical annealing (ICA) temperatures followed by air cooling to the bainitic region then air cooled to RT. Heating/cooling schedules are shown below in Table 3.2. Temperatures were measured via thermocouples placed into the steel specimens. Cooling rates involved the steel being extracted from the ovens and held at room temperature until placed back into an oven. The cooling rates were approximately 8.5^{o}C/s from full austenization to the intercritical region. From the intercritical region to the bainitic region, cooling rates were determined to be approximately 8.0^{o}C/s. XRD

procedures followed to obtain microstructural phase fractions for the different annealing cycles.

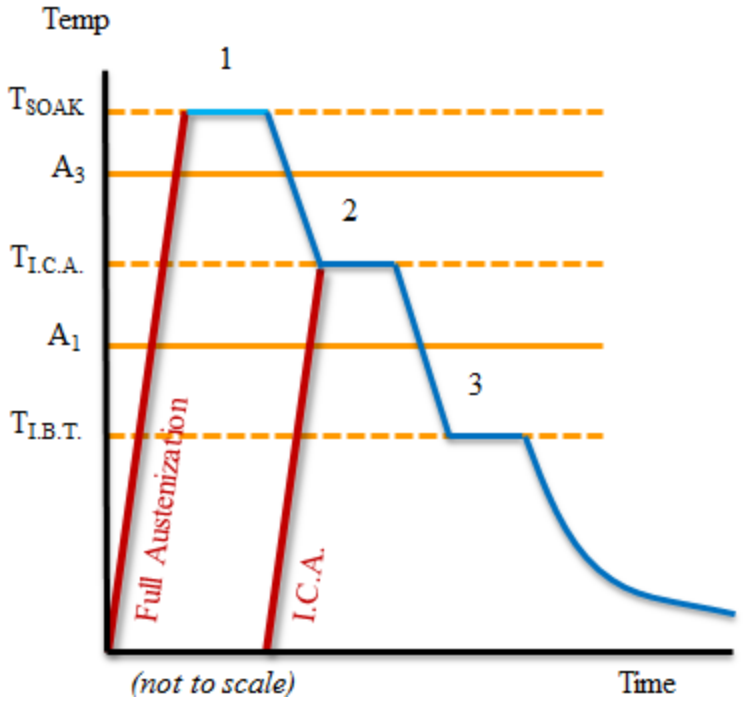

Figure 3.2 Heating/cooling schematic showing typical cooling schedules.

Table 3.2 Time specific heating/cooling schedule for treated TRIP steel.

	Case A	**Case B**	**Case C**
1. T_{SOAK} *(860°C)*	15 min.	0 min.	15 min.
2. $T_{I.C.A.}$ *(740°C)*	15 min.	15 min.	15 min.
3. $T_{I.B.T.}$ *(430°C)*	5 min.	5 min.	10 min.

The case that suggested the largest difference in mechanical behavior was used to recreate quasi-static and high strain-rate testing specimens to observe the responses to the respected tests. These tests were carried out through the following protocols: no baking

or pre-strain (comparable to as-received TRIP680), 2% pre-strained and baked, and 5% pre-strained and baked. XRD followed to determine austenite transformation percentages of each.

3.3 Results and Discussion

3.3.1 Examination of the Microstructure, Chemical Composition, and Microhardness of the As-received TRIP680

Chemical composition from the as-received TRIP680 was determined via chemical spectroscopy with the results shown in Table 3.3. The purpose of obtaining the chemical composition was for the derivation of phase and CCT diagrams aimed at developing heating/cooling schedules for re-annealing procedures. Microstructural images, shown in Figure 3.3, were used to determine bainite volume fractions. As-received bainite fractions were shown to be 39.0%

Table 3.3 Chemical composition of as-received TRIP680.

C	Si	Mn	P	S	Cr	Mo	Al	V	Nb
0.206	0.056	1.54	0.011	0.005	0.019	0.0038	0.93	0.0035	<0.004

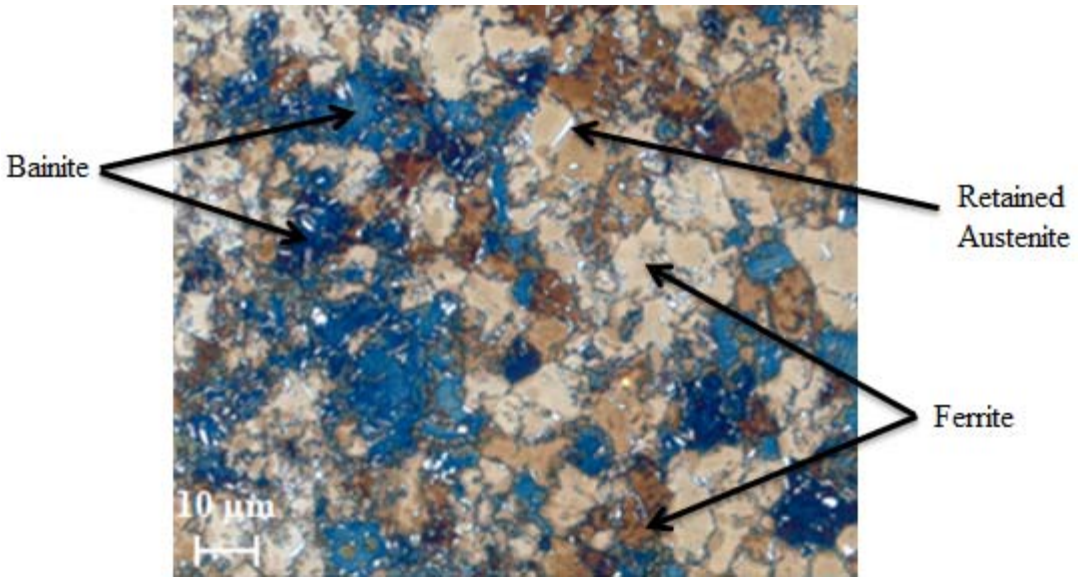

Figure 3.3 TRIP680 etched with Beraha's tint etchant: ferrite (tan and dark brown), bainite (blue), and retained austenite (bright white).

XRD analysis was performed on the as-received TRIP680. Figure 3.4 shows the results from the XRD scan on the analysis. The (110) and (310) curves were used to calculate the percentages of ferrite and austenite, respectively. Results of the analysis through the direct comparison method gave a 0.447:1 ratio of retained austenite to ferrite [23]. Knowing that the bainite fraction was 39.0%, overall ferrite and austenite fractions were calculated to be 41.4% ferrite and 19.6% retained austenite.

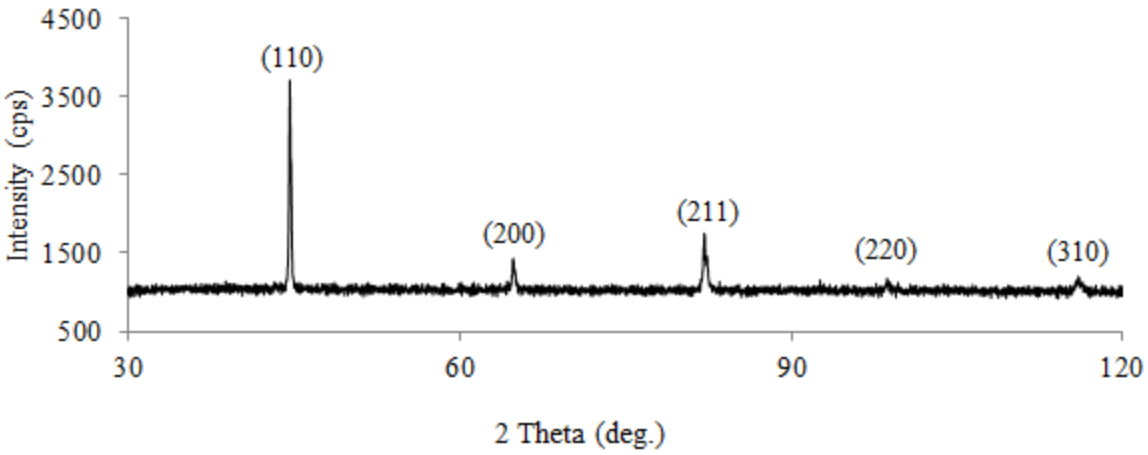

Figure 3.4 XRD scan from as-received TRIP680.

Vickers tests were performed on the as-received TRIP680 after etching with Beraha's tint etchant. Figure 3.5 shows images from indenting on to the steel. Ferrite and bainite phases were indented to investigate the hardness of the two phases. The austenite grains were not large enough to completely encase the indenter head. For this reason, austenite hardness values were not investigated. Hardness results from the tests for bainite and ferrite were 240.0 Hv and 207.8 Hv, respectively.

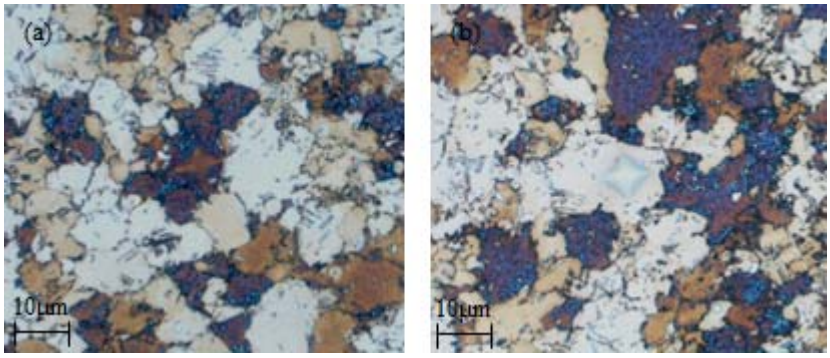

Figure 3.5 Optical microscopy showing Vickers indents on (a) bainite and (b) ferrite.

3.3.2 Investigation into the Thermo-mechanical Preconditioning Effects on the Mechanical Behavior of As-received TRIP680

Quasi-static tensile tests were performed and shown in Figure 3.6. Specimens were preconditioned according to the test schedule in Table 3.1. There were variations of responses resulting from the implemented work-hardening. However, the 2% pre-strained and baked specimens revealed the highest UTS at 813.8 MPa. Lower applied strain rates were able to reach higher UTS at longer elongations. In the lower strain-rate tests, a small dip near yield is observed where phase transformation may take place. Yield for the 5% pre-strained and baked specimens occurred much higher than the other test conditions.

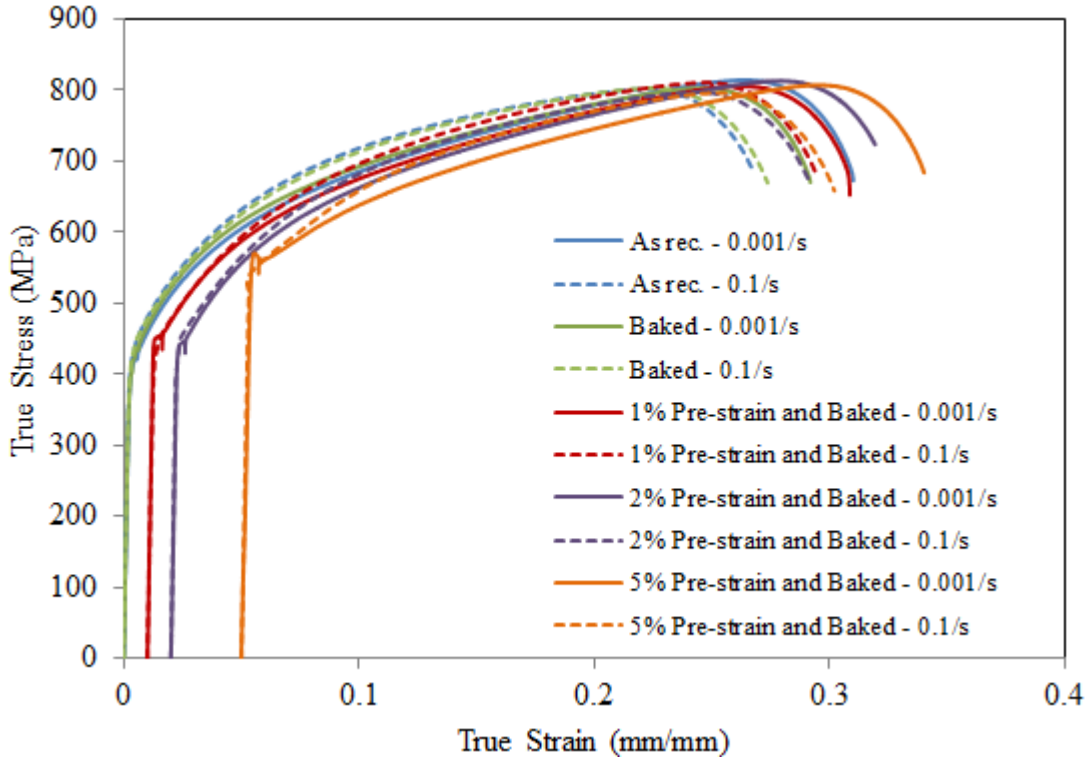

Figure 3.6 True stress vs. true strain curves resulting from quasi-static tensile tests.

Thermo-mechanical response characteristics can be determined from the quasi-static results shown above. Of those, Figure 3.7 shows the work-hardening characteristics from the (a) 0.1/s strain-rate and (b) 0.001/s strain-rate. For the 0.001/s case, there was only a subtle increase of the work-hardening characteristics from 1% to 2% pre-strains (from 9 to 18 MPa, respectively), but from 2% to 5% there was an increase of over 90 MPa of the work-hardening index reaching an overall effect of 110 MPa. This signals that the extra pre-strain from 2% to 5% creates a significant increase in yield strength possibly from a transition of austenite to martensite occurring during the 5% pre-strain. As was the case for the 0.1/s case, the 0.001/s tests showed the 5% pre-strain to cause much higher work-hardening characteristics that resulted in an increased yield of over 150 MPa.

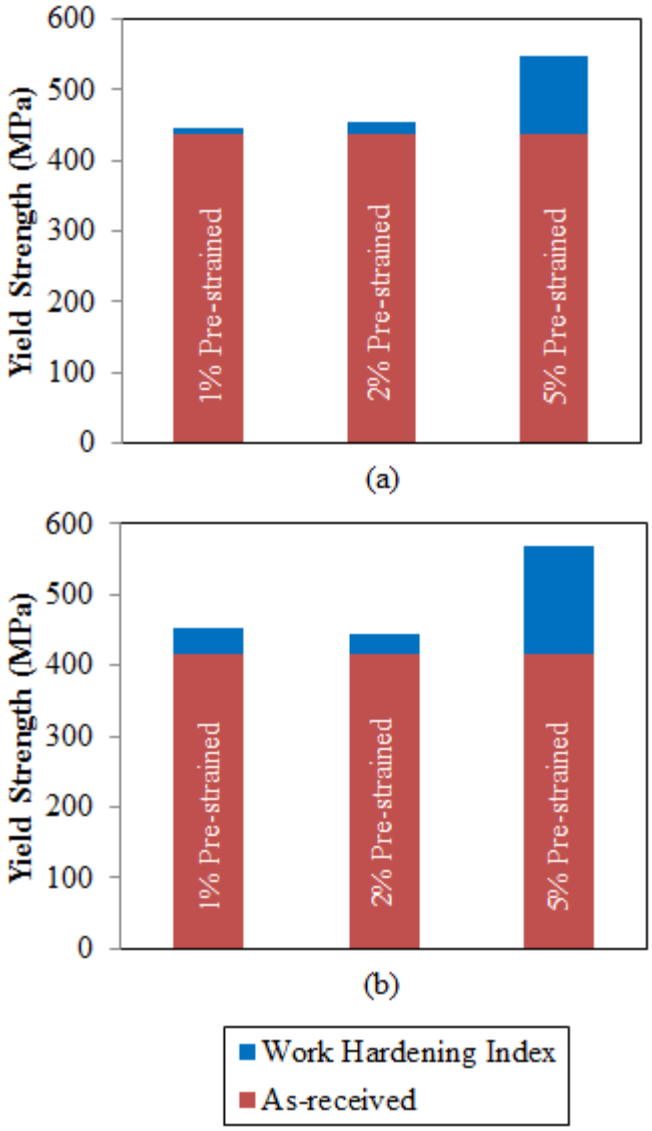

Figure 3.7 Work-hardening indices with respect to various thermo-mechanical preconditioning protocols.

Notes: (a) – 0.1/s strain rate, (b) – 0.001/s strain rate.

Quasi-static test fractography with SEM reveals fracture modes with very limited dimpling fracture surfaces at all strain rates. For the specimens tested at 0.1/s, smaller pre-strains exuded more predominant the cup-and-cone fracture surface with cleave planes spanning the width of the specimen at approximately 45^{o} to the direction of maximum stress shown in Figure 3.8 (a-b). The more intense pre-strains had cleavage

planes that began to grow from the center out on one side of the specimen (c,e). The 2% pre-strain and baked specimen appeared to have the most brittle fracture surface which corresponds to it having the highest UTS. The cup-and-cone fracture surfaces correspond in fact to shear banding at the planes with maximum stresses.

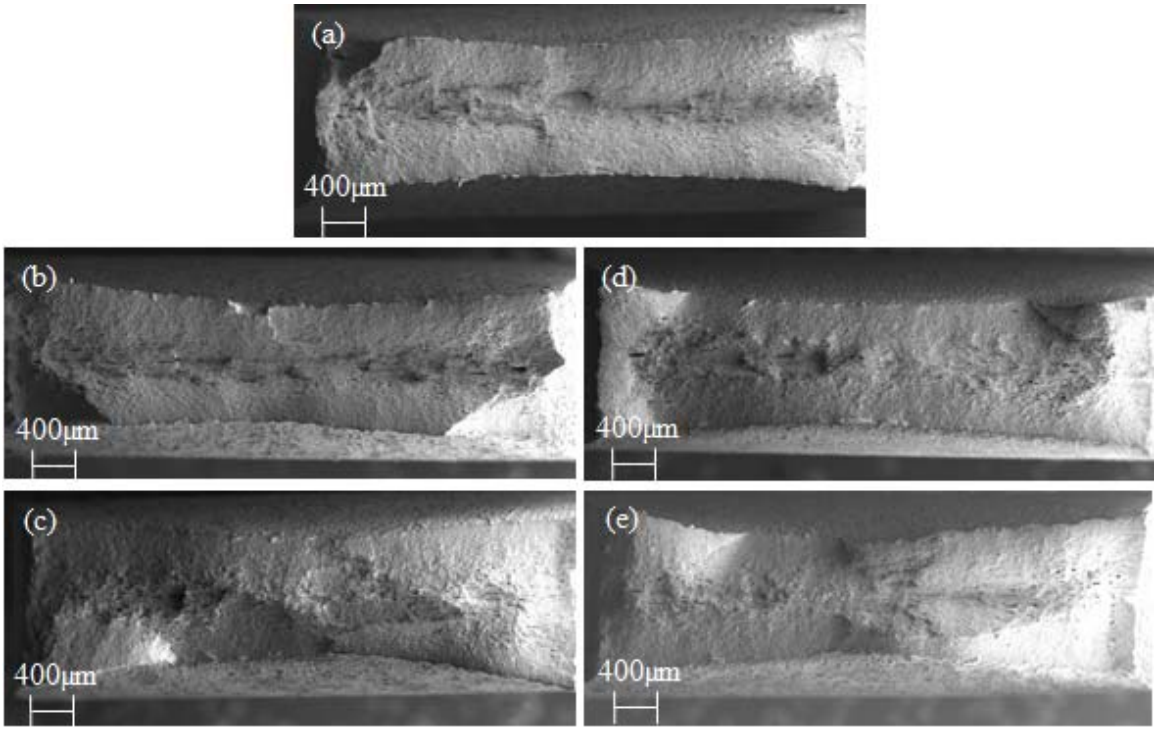

Figure 3.8 Fractography of specimens from quasi-static testing tested at 0.1/s strain rate.

Note: (a) as received, (b) baked, (c) 1% pre-strain and baked, (d) 2% pre-strain and baked, (e) 5% pre-strain and baked.

The fractography specimens tested at 0.001/s strain rates appeared to have the nearly the opposite results as seen in Figure 3.9. The specimens with no pre-strain showed the cleavage planes growing from the middle edge of the specimen (a-b), where the specimens with 1% and 2% pre-strains appeared more brittle with fracture planes in the corners (c,e). This is probably due to the higher fraction of TRIP-induced martensite

before baking. The baking process should have tempered the deformed martensite by forming carbides in the lath boundaries. This may have most likely induced tempering embrittlement with an increase tendency to nucleate shear bands early in post-testing. In fact, the specimen pre-strained to 5% showed a much higher reduction of ductility which does not complete the required elongation as compared to the specimen pre-strain to 1% and 2%. This indicates a higher tendency to shear localization. As in the 0.1/s series, the 2% pre-strained and baked specimen appeared different than the rest of the specimens (d). In this case, the fracture surface may suggest that the shear nucleated from the center of the specimen. However, the most plausible explanation is that the shear band nucleated at the free-surface and then intersected at the center of the specimen to induce a tensile stress state with the high hydrostatic pressure. This is why damage seems to be more pronounced near the central regions of the fractured specimens.

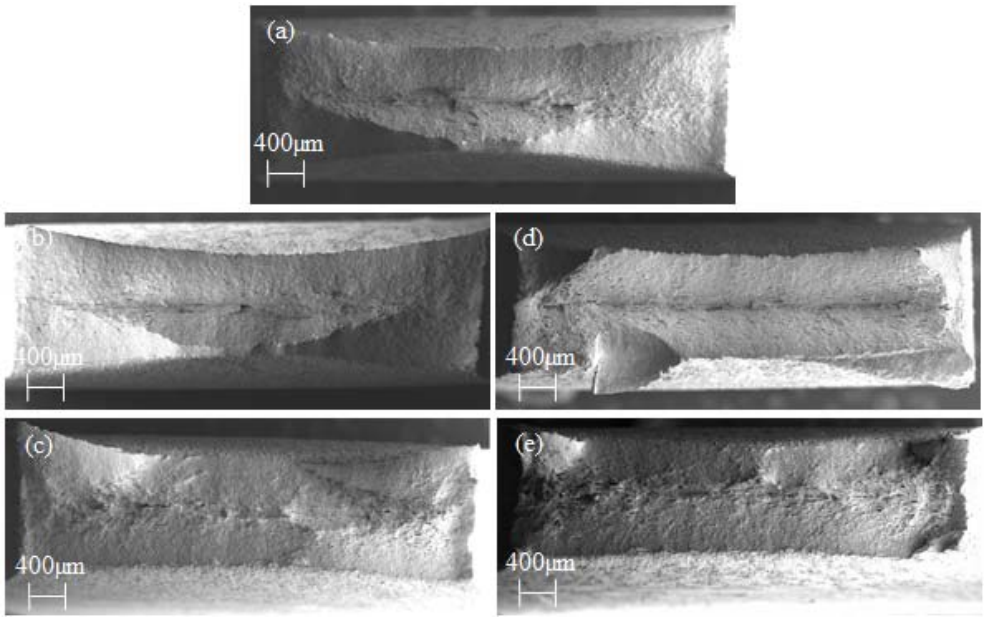

Figure 3.9 Fractography of specimens from quasi-static testing tested at 0.001/s strain rate.

Note: (a) as-received, (b) baked, (c) 1% pre-strain and baked, (d) 2% pre-strain and baked, (e) 5% pre-strain and baked.

High strain-rate tests, shown in Figure 3.10, were performed with the intent of observing the mechanical response during high-speed strains to more adequately represent a more typical automotive collision. The test parameters used here were the same that were used under the quasi-static testing regime. Regarding yield, there was negligible baking effect. The 2% and 5% pre-strain cases had the most noticeable trends differing from the as-received series. Comparing the high strain-rate results to the quasi-static results, negative strain rate sensitivity is evident due to the higher maximum tensile stresses in all cases but the as-received material. Every other test displayed higher tensile stresses in the high strain-rate regime than in the quasi-static.

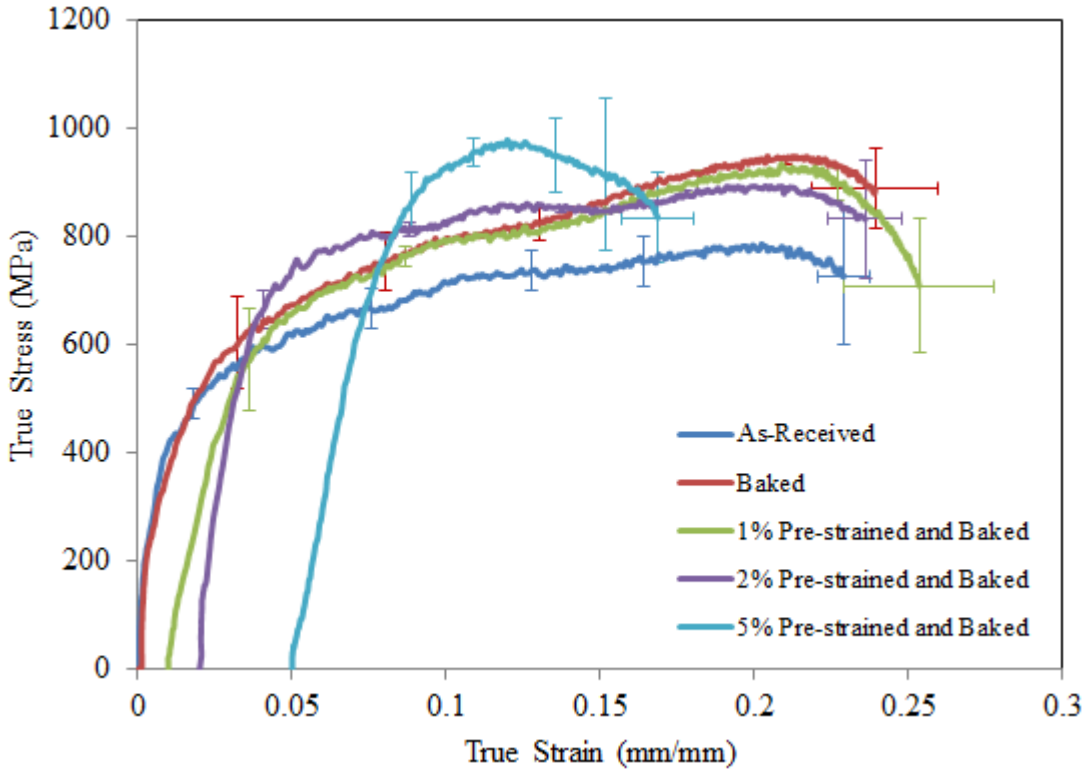

Figure 3.10 True stress vs. true strain graph resulting from high strain rate tensile tests.

3.3.3 Heat-Treating and the Resultant Microstructural and Mechanical Observations

Heating/cooling treatments were carried out with the desire of altering the phase fractions of retained austenite for the purpose of further testing and response comparisons. Optical microscopic images were taken of the I.C.A. treated series in order to observe the bainite fractions seen in Figure 3.11. The specimen was etched with Beraha's color etch and viewed with a Zeiss Axiovert 200 optical microscope. The resultant bainite fractions were found to be 21.3% from image analysis software.

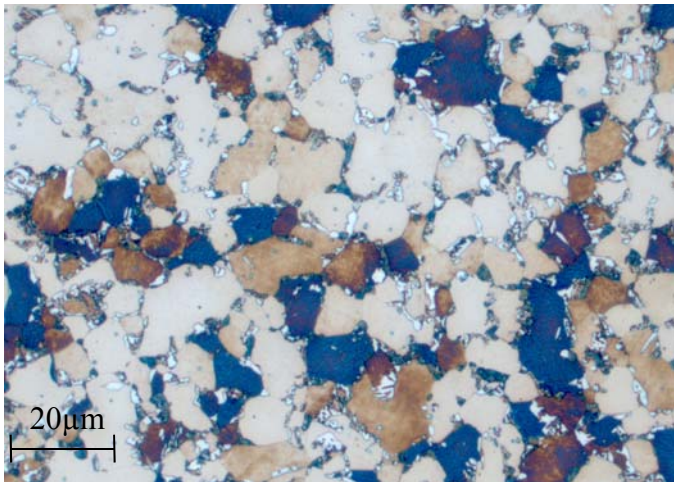

Figure 3.11 I.C.A. heat-treated TRIP steel showing the three phases of the steel: ferrite (tan and brown), bainite (blue), and retained austenite (bright white).

XRD was used to verify the amount of retained austenite. Figure 3.12 shows the results from the XRD analysis. The peaks were indexed into five different Miller indices representing the ferrite and austenite in the microstructure of the steel. Through image analysis with Beraha's color etching and the direct comparison method [23], volume fractions were calculated for the comparison of the as-received TRIP680 to the heat-treated steels. Table 3.4 shows the results of the phase fractions in the steel. The I.C.A. heating procedure provided the greatest contrast of hypothesized mechanical behavior

compared to the original TRIP680 series due to the increased ferrite volume and decreased bainite volume. Therefore, this procedure will be used in mechanical testing to compare the mechanical and microstructural response with the as-received series.

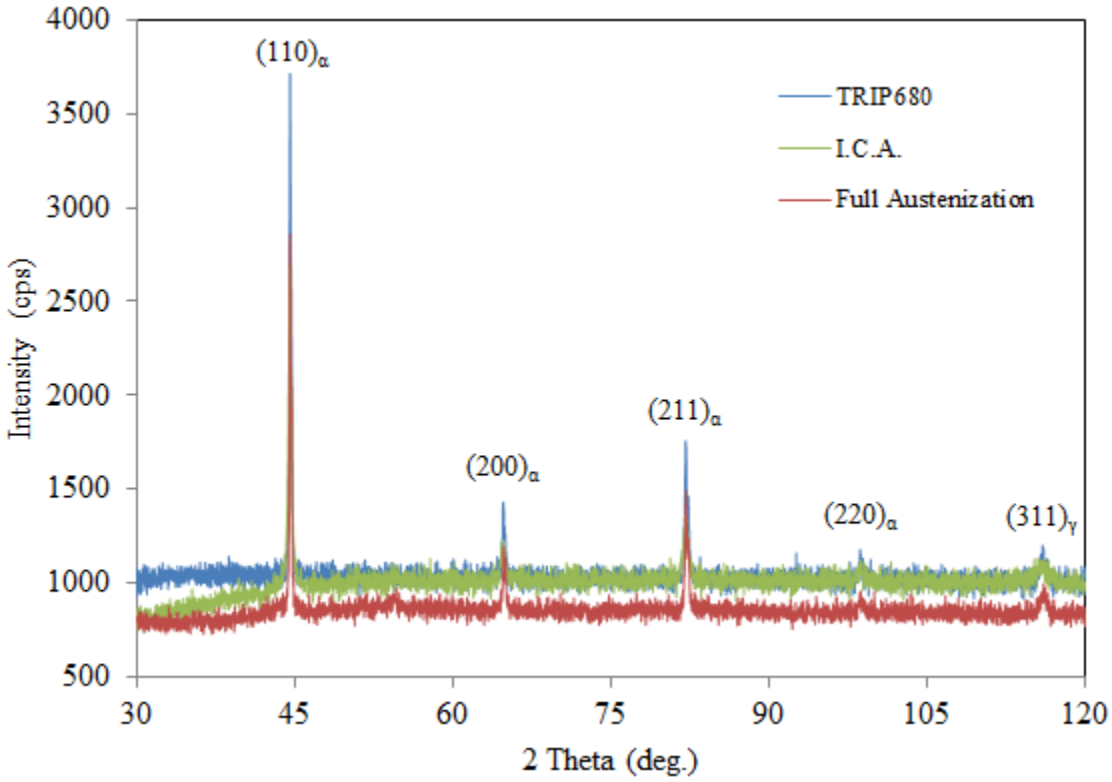

Figure 3.12 XRD Analysis of the TRIP steel series with the five major absorption peaks indexed.

Table 3.4 Phase volume fraction results of the as-received condition compared with the heat treated series.

	Phase Fractions (vol. %)		
TRIP Series	*Ferrite*	*Bainite*	*Austenite*
As-Received	41.4	39.0	19.6
Full Austenization	43.5	32.7	23.8
I.C.A.	62.2	21.3	16.5

Quasi-static tensile tests were performed on the newly created I.C.A. steel in at 0.1/s strain-rate under three preconditioning protocols: no pre-strain, 2% pre-strain and baked, and 5% pre-strain and baked. Comparisons of that and the original TRIP680 are shown in Figure 3.13. As anticipated, the I.C.A. series performed weakly compared to the as-received series likely due to the smaller percentage of bainite and retained austenite. In the case of the I.C.A. with no pre-strain and 2% pre-strain, the retained austenite-to-martensite transformation can be seen right after yielding. The more horizontal action of the respective stress-strain curves illustrates the mechanical behavior during phase transformation. However, the 5% pre-strained-and-baked series did not display this behavior alluding to most of the martensitic transformation occurring during the 5% pre-straining.

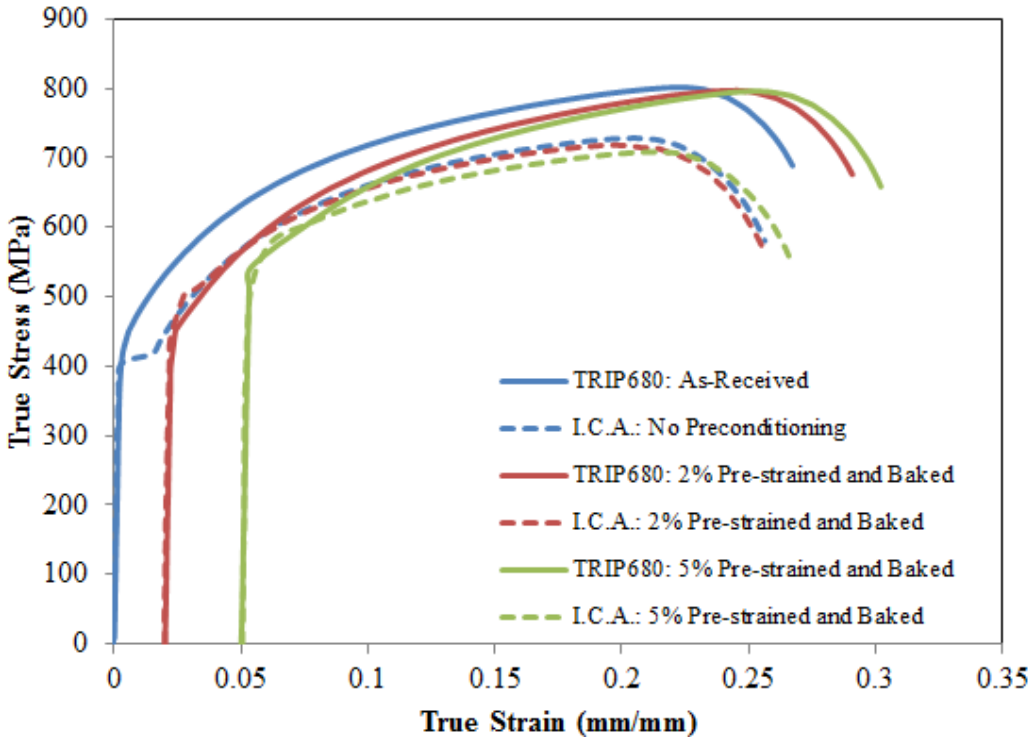

Figure 3.13 Quasi-static stress vs. strain results comparing the received TRIP680 to the I.C.A. series under three different preconditioning protocols.

The fractured specimens were subjected to XRD scans and then analyzed through the direct comparison method. Figure 3.14 shows the scan of the as-received 5% pre-strained and baked specimen. Peaks of the existing ferrite and austenite microstructure are labeled. In addition, newly formed martensitic peaks are highlighted in red. The results of the scan showed an existing volume fraction of 7.3±0.6% retained austenite. This suggests that over 60% of the austenite transformed to martensite. All of the quasi-static XRD results followed this trend.

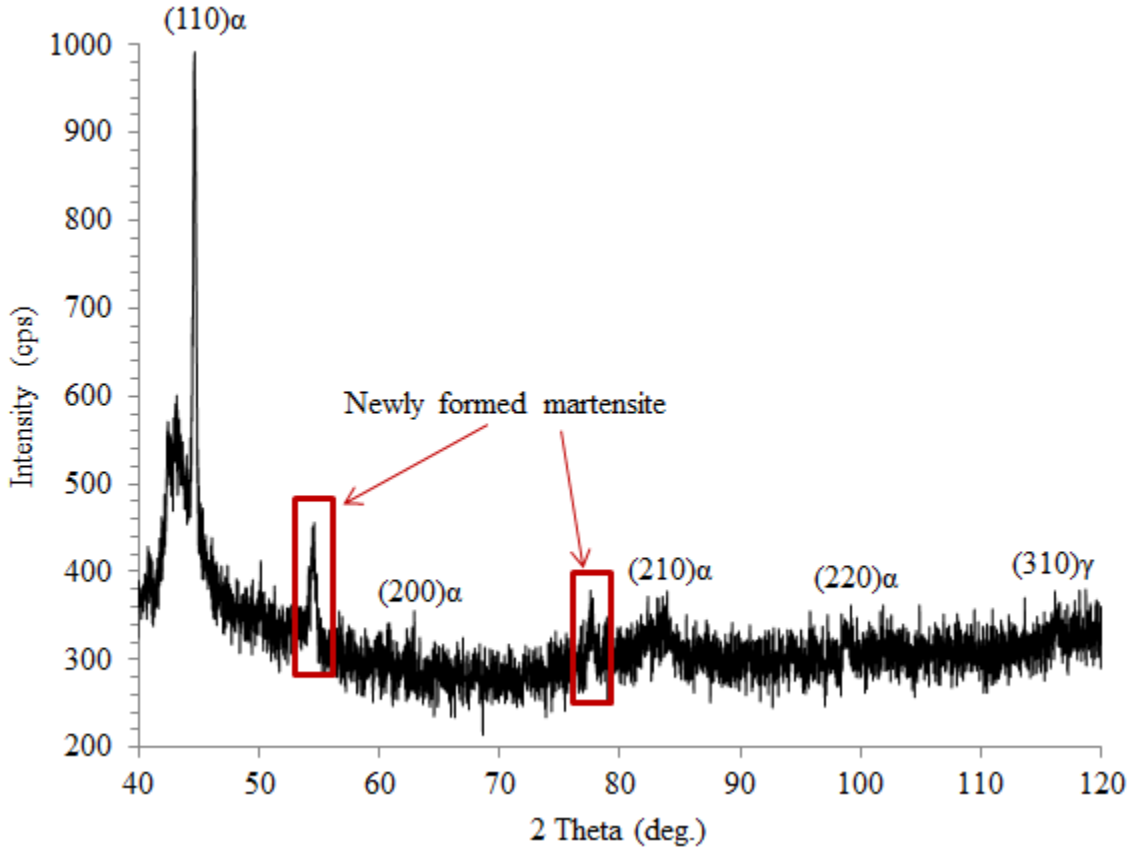

Figure 3.14 XRD Analysis of the TRIP steel series with the five major absorption peaks indexed.

Figure 3.15 shows fractographical images that were taken via SEM from the quasi-static tensile tests on the I.C.A. series. As with the as-received specimens, the 5%

pre-strained and baked of the I.C.A. case displayed a large reduction in elongation compared to the I.C.A. specimen with no pre-conditioning (c and a, respectively). This alludes to shear localization occurring with this series as well. The trend of higher martensite content in each specimen with increased pre-strains is almost surely another factor in why the elongation is reduced in both the 2% and 5% specimens.

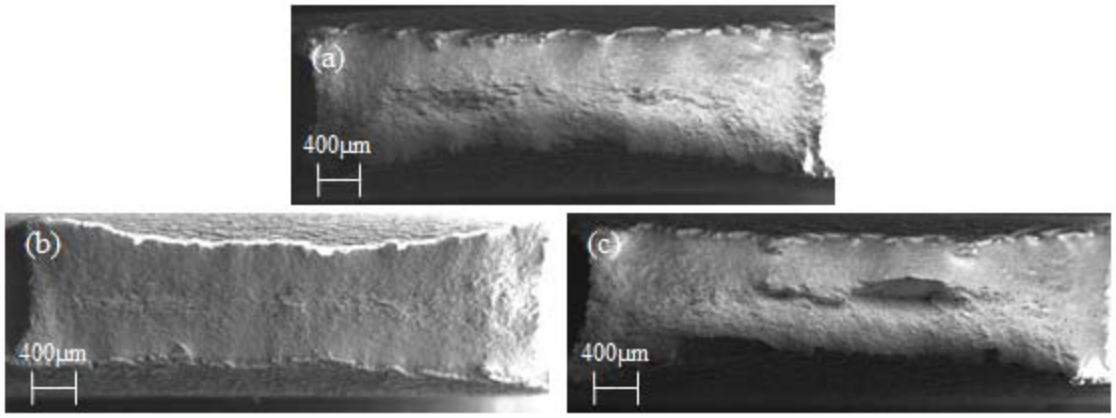

Figure 3.15 Fractographical images from the I.C.A. series following quasi-static testing.

Note: (a) No pre-strain or baking; (b) 2% pre-strain and baking; (c) 5% pre-strain and baking.

High strain-rate tensile tests shown in Figure 3.16 were performed on the I.C.A. series in order to observe the mechanical behavior of the steel subjected to strain at high speeds and to provide a comparison to the behavior of the TRIP680 (Fig. 3.13). Due to the increase of the ferrite fraction and as a result ductility, the I.C.A. series behavior was comparable to the quasi-static tests in comparison to the received TRIP680. However, in the high strain-rate tests, the I.C.A. specimens displayed much more elongation to failure when compared to the TRIP680 than was observed in the quasi-static tests. Therefore,

since the majority of failures of an automotive body are in high strain-rate environments, the high strain-rate testing would be the most important case to note in this investigation.

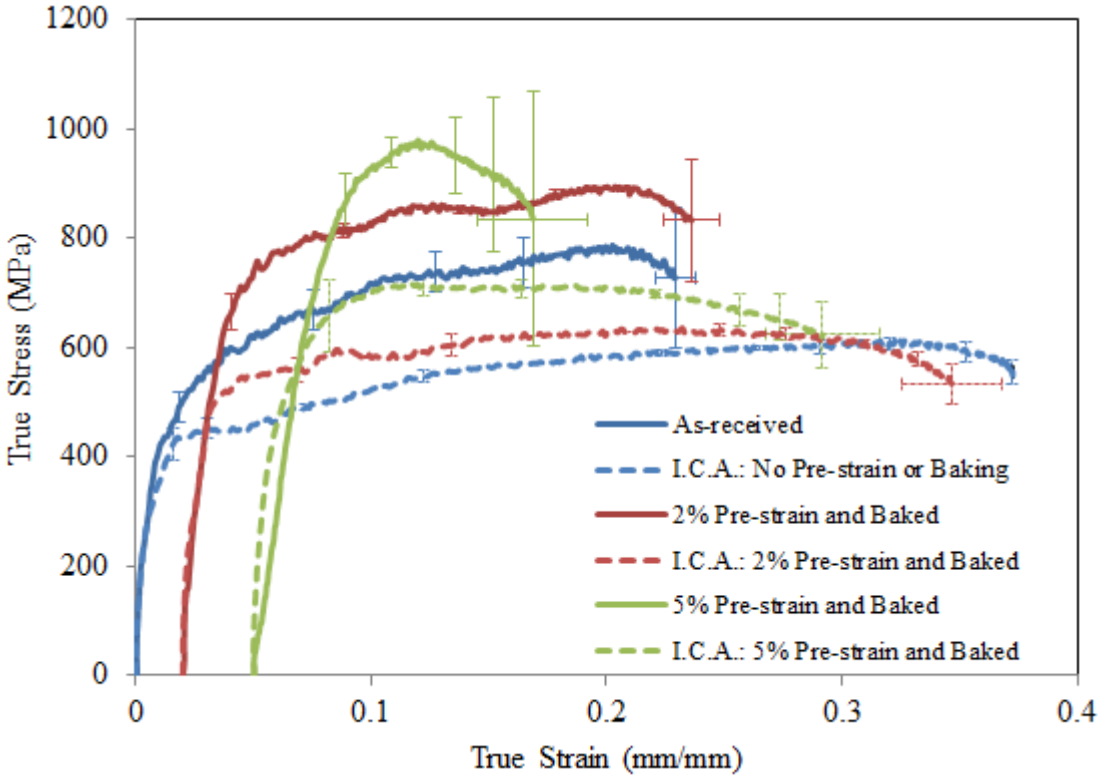

Figure 3.16 True stress vs. true strain graph resulting from high strain-rate tensile tests of the I.C.A. series.

The high strain-rate fracture specimens were subjected to XRD scans and then analyzed through the direct comparison method. Figure 3.17 shows the scan of the as-received 5% pre-strained and baked specimen. The martensitic peaks are highlighted while no (310) peaks are evident. Therefore, the XRD analysis alludes to complete austenitic transformation. All of the high strain-rate XRD results followed this trend.

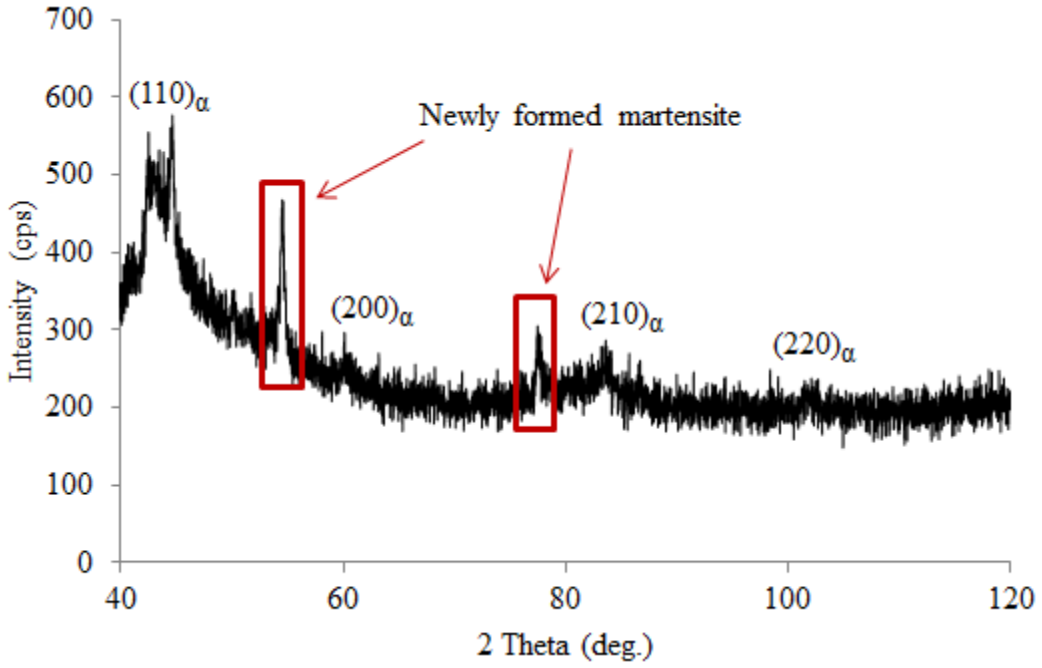

Figure 3.17 XRD Analysis of the TRIP steel series with the five major absorption peaks indexed.

CHAPTER IV

CONCLUSION

4.1 DP Steel Conclusions

Baking effects were observed to have a profound effect in every test case except for 5% pre-strained cases. This proves that once the material reaches this strain, the dislocations caused by the higher strain refuse to allow carbon atoms diffused into the steel to have any major role in increasing strength.

The microstructure variation of DP steel caused by altered cooling patterns drastically affects the behavior of the material by varying the amounts of martensite and ferrite in the steel. Different variations of the cooling parameters here were used to obtain the two combinations that offered the largest contrast in phase fractions, one having a high percentage of ferrite and one having a high percentage of martensite. Quasi-static and high strain-rate tensile tests showed a much higher ultimate tensile strength when the steel contained the most martensite. However, elongation to failure, thus the formability, was greatly reduced. The steel containing the most softer-phase ferrite had just the opposite effect. Elongation was increased slightly but a lower strength was observed.

4.2 TRIP Steel Conclusions

The received TRIP680 had an initial phase fraction of 42% ferrite, 39% bainite, and 19% retained austenite. Baking effects were proved not to have a significant consequence on the outcome of the strength and elongation in quasi-static testing.

However, work-hardening had a major effect on the strength of the material. The increase in yield strength from 2% pre-strain to 5% pre-strain was very substantial alluding to the austenite transforming into martensite rapidly somewhere between these strain values. High strain-rate testing confirmed this as well. There was also a rise in yield from just adding 1% and 2% pre-strain, but not to the extent of the 5% pre-strain. XRD analysis revealed that 60% of the total austenite fraction is transformed into martensite during quasi-static testing. Under high strain-rate testing, there was no evidence of a $(310)_\gamma$ peak signaling that complete transformation had taken place under these more extreme testing conditions.

The intercritical annealing method was used to re-create the TRIP steel with a phase composition of 62.2% ferrite, 21.3% bainite, and 16.5% retained austenite. The increased ferrite percentage and decreased bainite percentage reduced the strength of the steel of approximately 9%. The increase of elongation-to-failure was seen in high strain-rate tests. High strain-rate testing revealed a decrease of strength of over 30%. These high strain-rate tests amplified the difference in the two steels much more than the slower, quasi-static testing.

REFERENCES

[1] Z. G. Hu, P. Zhu, and J. Meng, "Fatigue Properties of Transformation-induced Plasticity and Dual-phase Steels for Auto-body Lightweight: Experiment, Modeling, and Application," *Materials and Design*, vol. 31, pp. 2884–2890, 2010.

[2] J. Van Slycken, P. Verleysen, J. Degrieck, L. Samek, and B. C. De Cooman, "High-Strain-Rate Behavior of Low-Alloy Multiphase Aluminum- and Silicon-Based Transformation-Induced Plasticity Steels," *Metallurgical and Materials Transactions*, vol. 37, pp. 1527–1539, 2006.

[3] R. O. Rocha, T. M. F. Melo, E. V. Pereloma, and D. B. Santos, "Microstructural Evolution at the Initial Stages of Continuous Annealing of Cold Rolled Dual-Phased Steel," *Mat. Sci. Eng.*, vol. 391, pp. 296–304, 2005.

[4] M. Sarwar and R. Priestner, "Influence of Ferrite-Martensite Microstructural Morphology on Tensile Properties of Dual-phase Steel," *Journal of Materials Science*, vol. 31, pp. 2091–2095, 1996.

[5] W. J. Dan, W. G. Zhang, S. H. Li, and Z. Q. Lin, "A Model for Strain-induced Martensitic Transformation of TRIP Steel with Strain Rate," *Comp. Mater. Sci.*, vol. 40, pp. 101–107, 2007.

[6] Z. Morita, T. Emi, T. Enami, and O. Hashimoto, "An Introduction to Iron and Steel Processing," 21st Century Steel Foundation, 1997.

[7] World Auto Steel, "Advanced High Strength Steel Application Guidelines." International Iron and Steel Institute, Mar-2009.

[8] Y. Sakuma, S. Itami, O. Kawano, N. Kimura, S. Hiwatashi, and K. Sakata, "Next-Generation High-Strength Sheet Steel Utilizing Transformation-Induced Plasticity Effect," Nippon Steel, 64, Mar. 1995.

[9] J. Lis, A. K. Lis, and C. Kolan, "Processing and Properties of C-Mn Steel with Dual-Phase Microstructure," *Journal of Mat. Proc. Tech.*, vol. 162–163, pp. 350–354, 2005.

[10] M. Erdogan, "The Effect of New Ferrite Content on the Tensile Fracture Behavior of Dual Phase Steels," *Journal of Materials Science*, vol. 37, pp. 3623–3630, 2002.

[11] I. Timokhina, E. V. Pereloma, S. P. Ringer, R. K. Zheng, and P. D. Hodgson, "Characterization of the Bake-hardening Behavior of Transformation Induced Plasticity and Dual-phase Steels Using Advanced Analytical Techniques," *ISIJ Int.*, vol. 50, no. 4, pp. 574–582, 2010.

[12] M. R. Berrahmoune, S. Berveiller, K. Inal, A. Moulin, and E. Patoor, "Analysis of the Martensitic Transformation at Various Scales in TRIP Steel," *Mat. Sci. Eng.*, vol. 378, pp. 304–307, 2004.

[13] D. Herring, "A Discussion of Retained Austinite," *Industrial Heating*, pp. 14–16, Mar. 2005.

[14] A. Basuki and E. Aernoudt, "Effect of Deformation in the Intercritical Area on the Grain Refinement of Retained Austeninte of 0.4C TRIP Steel," *Scripta Materialia*, vol. 40, no. 9, pp. 1003–1008, 1999.

[15] V. F. Zackay, E. R. Parker, D. Fahr, and R. Busch, "The Enhancement of Ductility in High-Strength Steels," *ASM Trans Quart.*, vol. 60, no. 2, pp. 252–259, 1967.

[16] T. Senuma, "Physical Metallurgy of Modern High Strength Steel Sheets," *ISIJ Int.*, vol. 41, no. 6, pp. 520–532, 2001.

[17] S. Yasuki, K. Sugimoto, M. Kobayashi, and S. Hashimoto, "Low Cylce Fatigue-Hardening of TRIP-Aided Dual Phase Steels."

[18] Y. Tomita and T. Iwamoto, "Constitutive Modeling of TRIP Steel and Its Application to the Improvement of Mechanical Properties," *Int. J. Mech. Sci.*, vol. 37, no. 12, pp. 1295–1305, 1995.

[19] P. Jacques, Q. Furnemont, T. Pardoen, and F. Delannay, "On the Role of Martensitic Transformation on Damage and Cracking Resistance in TRIP-Assisted Multiphase Steels," *Acta Mater.*, vol. 49, pp. 139–152, 2001.

[20] G. H. Staab and A. Gilat, "A Direct-tension Split Hopkinson Bar for High Strain-rate Testing," *Experimental Mechanics*, vol. 31, no. 3, pp. 232–235, Sep. 1991.

[21] V. Savic, L. G. Hector, Jr., and J. R. Fekete, "Digital Image Correlation Study of Plastic Deformation and Fracture in Fully Martensitic Steels," *Experimental Mechanics*, vol. 50, pp. 99–110, 2010.

[22] "Metals Handbook," ASM International, 1990.

[23] B. D. Cullity, *Elements of X-Ray Diffraction*, Second. Addison-Wesley Publising Company, Inc., 1978.

[24] B. L. Averbach and M. Cohen, “X-ray Determination of Retained Austenite by Integrated Intensities,” *Trans. AIME*, vol. 176, p. 401, 1948.

APPENDIX A

CULLITY'S DIRECT COMPARISON METHOD

A.1 Theory of Direct Comparison Phase Fraction Analysis

Since the direct comparison method does not require a pure phase material, this analysis technique to the XRD results is a solid method in determining phase volume fraction in multi-phase materials with crystalline phases. Averbach and Cohen developed this method and since then it has been widely used for determining retained austenite in hardened steel [24]. The methodology presented here is similar to that shown in Cullity's Elements of X-ray Diffraction.

$$K_2 = \left(\frac{I_0 \cdot A \cdot \lambda^3}{32\pi r}\right) \cdot \left[\left(\frac{u_o}{4\pi}\right) \cdot \frac{e^4}{m^2}\right] \tag{A. 1}$$

$$R = \left(\frac{1}{v^2}\right)\left[(|F|)^2 \cdot p \cdot \left(\frac{1+\cos^2 2\theta}{\sin^2\theta \cdot \cos\theta}\right)\right] \cdot \left(e^{-2M}\right) \tag{A. 2}$$

Note: K2 = a constant, independent of the kind and amount of the diffracting substance, R = value dependent on θ, *hkl*, and kind of substance, I_o = intensity of incident beam, A = cross-sectional area of incident beam, λ = wavelength of incident beam, r = radius of diffractometer, $\mu_o = 4\pi \times 10^{-7}$ m kg C^{-2}, e = charge on electron, m = mass of electron, v = volume of unit cell, F = structure factor, p = multiplicity factor, θ = Bragg angle, e^{-2M} = temperature factor, and

Some of these variables have no influence on the output of the ratio of the austenite to ferrite ratio because they would be the same for both phases. Therefore, these variables can be ignored in the equations. These variables are λ, r, μ_o, e, m, e^{-2M} (check Mathcad files for more). Next, the diffracted intensity equation is shown in A. 3:

$$I = \frac{K_2 \cdot R}{2\mu} \tag{A. 3}$$

Note: I = integrated intensity per unit length of diffraction line and μ = linear absorption coefficient.

Then by designating austenite by the subscript γ and ferrite by the subscript α, each equation can be written as:

$$I_\gamma = \frac{K_2 \cdot R\gamma \cdot c_\gamma}{2\mu_m} \tag{A. 4}$$

$$I_\alpha = \frac{K_2 \cdot R_\alpha \cdot c_\alpha}{2\mu_m} \tag{A. 5}$$

Note: μ_m is the is the linear coefficient of the mixture and c is the concentration of the phase.

However, to find the ratio of austenite to ferrite, division of these equations produces:

$$\frac{I_\gamma}{I_\alpha} = \frac{R_\gamma \cdot c_\gamma}{R_\alpha \cdot c_\alpha} \tag{A. 6}$$

A.2 Example of Direct Comparison Method – As-received TRIP680 Analysis

- Since ratios are the end goal in mind, units are unnecessary.
- Given (for calculation purposes, $x = e^{-2M}$)

$\lambda := 1.54 \cdot 10^{-10}$ $\mu_o := 4 \cdot \pi \cdot 10^{-7}$ $r := 0.3$ $\mu := 304.4$

$e := -1.602 \cdot 10^{-19}$ $u := 304.4$ $m := 9.109 \cdot 10^{-31}$ $A := 1 \cdot 10^{-5}$

$r_{Fe} := 140 \cdot 10^{-12}$

- For the (110) peak:
    - The volume of the BCC ferrite crystal:

$$v_{bcc} := \left(\frac{4r_{Fe}}{3^{.5}}\right)^3 \qquad v_{bcc} := 3.379 \cdot 10^{-29} \tag{A. 7}$$

- Variables at time of testing:

$\theta := 22.28\text{deg} \quad x := 0.96 \quad I_o := 3707 \quad p := 12$

$f := 20.75 \quad F := 2 \cdot f = 41.5$

- The calculation of K_2 and R:

$$K_2 := \left(\frac{I_o \cdot A \cdot \lambda^3}{32 \cdot \pi \, r}\right) \cdot \left[\left(\frac{\mu_o}{4\pi}\right)^2 \cdot \frac{e^4}{m^2}\right] = 3.563 \times 10^{-62} \tag{A. 8}$$

$$R := \left(\frac{1}{v_{bcc}^{\,2}}\right) \cdot \left[(|F|)^2 \cdot p \cdot \left(\frac{1 + \cos(2\theta)}{\sin(\theta)^2 \cdot \cos(\theta)}\right) \cdot x\right] = 2.237 \times 10^{62} \tag{A. 9}$$

- Calculation of I:

$$I := \frac{K_2 \cdot R}{2u} = 0.013 \tag{A. 10}$$

- For the (310) peak:
  - The volume of the BCC ferrite crystal:

$$v_{fcc} := \left(\frac{4r_{Fe}}{2^{.5}}\right)^3 \qquad v_{fcc} := 6.209 \cdot 10^{-29} \tag{A. 11}$$

  - Variables at time of testing:

$\theta := 58.04\text{deg} \quad x := .81 \quad I_o := 1202 \quad p := 48$

$f := 9.75 \quad F := 4 \cdot f$

  - The calculation of K_2 and R:

$$K_2 := \left(\frac{I_o \cdot A \cdot \lambda^3}{32 \cdot \pi \, r}\right) \cdot \left[\left(\frac{\mu_o}{4\pi}\right)^2 \cdot \frac{e^4}{m^2}\right] = 1.155 \times 10^{-62} \tag{A. 12}$$

$$R := \left(\frac{1}{v_{fcc}^{\,2}}\right) \cdot \left[(|F|)^2 \cdot p \cdot \left(\frac{1 + \cos(2\theta)}{\sin(\theta)^2 \cdot \cos(\theta)}\right) \cdot x\right] = 2.256 \times 10^{61} \tag{A. 13}$$

- Calculation of I:

$$I := \frac{K_2 \cdot R}{2u} = 4.282 \times 10^{-4} \quad \text{(A. 14)}$$

- Determining percentage of austenite in total ferrite and austenite phases:

$$\frac{I_\gamma}{I_\alpha} \cdot \frac{R_\alpha}{R_\gamma} = 0.322 \quad \text{(A. 15)}$$

- Finding total phase fraction of retained austenite (with 39% bainite):

$$0.322 \cdot (1 - 0.39) = 0.196 \quad \text{(A. 16)}$$

- Finding total phase fraction of ferrite (39% bainite, 19.6% ferrite):

$$1 - 0.196 - 0.39 = 0.414 \quad \text{(A. 17)}$$